

# Wavefront Estimation From a Single Measurement: Uniqueness and Algorithms

Nicholas Chimitt, *Member, IEEE*, Ali Almualllem, *Student Member, IEEE*,  
Qi Guo, *Member, IEEE*, Stanley H. Chan, *Senior Member, IEEE*

**Abstract**—Wavefront estimation is an essential component of adaptive optics where the goal is to recover the underlying phase from its Fourier magnitude. While this may sound identical to classical phase retrieval, wavefront estimation faces more strict requirements regarding uniqueness as adaptive optics systems need a unique phase to compensate for the distorted wavefront. Existing real-time wavefront estimation methodologies are dominated by sensing via specialized optical hardware due to their high speed, but they often have a low spatial resolution. A computational method that can perform both fast and accurate wavefront estimation with a single measurement can improve resolution and bring new applications such as real-time *passive* wavefront estimation, opening the door to a new generation of medical and defense applications.

In this paper, we tackle the wavefront estimation problem by observing that the non-uniqueness is related to the geometry of the pupil shape. By analyzing the source of ambiguities and breaking the symmetry, we present a joint optics-algorithm approach by co-designing the shape of the pupil and the reconstruction neural network. Using our proposed lightweight neural network, we demonstrate wavefront estimation of a phase of size  $128 \times 128$  at 5,200 frames per second on a CPU computer, achieving an average Strehl ratio up to 0.98 in the noiseless case. We additionally test our method on real measurements using a spatial light modulator. Code is available at <https://pages.github.itap.purdue.edu/St StanleyChanGroup/wavefront-estimation/>.

**Index Terms**—Wavefront estimation, wavefront sensing, adaptive optics, phase retrieval, neural representation

## I. INTRODUCTION

**I**MAGING systems are impacted by aberrations when a distorted wavefront is projected to a sensor, creating a less-than-ideal impulse response known as a point spread function (PSF). While image recovery can be done via post-processing, a commonly used hardware solution is adaptive optics (AO) which aims to cancel out the wavefront distortion in real-time and bring the system to its diffraction limit. The AO system has two tasks: wavefront estimation and correction. Ideally, we want to do wavefront estimation fast; if the distortion fluctuates in time, latency in estimation will reduce our ability to mitigate the effects due to phase decorrelation [1].

The authors are with the School of Electrical and Computer Engineering, Purdue University, West Lafayette, IN 47907, USA. Corresponding author: Nicholas Chimitt, email: [nchimitt@purdue.edu](mailto:nchimitt@purdue.edu).

The work is supported in part by the Intelligence Advanced Research Projects Activity (IARPA) under Contract No. 2022-21102100004, and in part by the National Science Foundation under the grants CCSS-2030570 and IIS-2133032. The views and conclusions contained herein are those of the authors and should not be interpreted as necessarily representing the official policies, either expressed or implied, of IARPA, or the U.S. Government. The U.S. Government is authorized to reproduce and distribute reprints for governmental purposes notwithstanding any copyright annotation therein.

This paper focuses on the estimation problem, i.e., recovering the wavefront from the PSF. We focus on the hardest limit: using only one *single* measurement. At the core of this problem is the recovery of the phase from a Fourier magnitude. This setting should be familiar to many readers who know phase retrieval. Indeed, wavefront estimation *is* a form of phase retrieval with a subtle but important difference. Both problems can be formulated as the recovery of a complex signal from its Fourier magnitude: if  $\mathbf{x} \in \mathbb{C}^N$  is the ground truth complex signal and  $\mathbf{F} \in \mathbb{C}^{M \times N}$  is an oversampled discrete Fourier transform matrix, then the inverse problem is to find  $\mathbf{x}$  from the measurement  $\mathbf{y} \in \mathbb{R}^M$  [2]–[7]:

$$\text{Find } \mathbf{x} \quad \text{subject to} \quad \mathbf{y} = |\mathbf{F}\mathbf{x}|^2. \quad (1)$$

However, because of the magnitude-square operation, the problem does not always have a unique solution.

The subtle but important difference between phase retrieval and wavefront estimation lies in the types of permissible ambiguous solutions of (1), divided into *trivial* and *non-trivial* ambiguities. As the names imply, trivial ambiguities are viewed as acceptable solutions to (1) in the context of phase retrieval [5]–[9]. The vast majority of phase retrieval papers is on eliminating non-trivial ambiguities.

The story is different for wavefront estimation. While wavefront estimation still suffers from the non-trivial ambiguity problem, there also exist trivial ambiguities that will severely degrade AO correction. Because of this, wavefront estimation is often performed by specialized optical hardware or, if done computationally, using multiple measurements [10], [11] to overcome the relevant trivial ambiguities.

### A. Why not just measure it?

If dealing with the trivial ambiguity is such an important but difficult problem, why don't we just *measure* the phase using a Shack-Hartmann wavefront sensor [1], [12]? Putting aside the cost (a typical setup from Thorlabs would cost thousands of dollars), the resolution is in the range of  $35 \times 21$  to  $73 \times 45$ . This means it cannot measure too many high-order aberrations, in addition it has been shown a Shack-Hartmann sensor can suffer when the aberrations are strong due to an effect analogous to crosstalk. Alternatives such as interferometry [13]–[15] can measure high-order aberrations, but are more suitable for laboratory settings due to their reliance on precise calibration.

Computational methods bring the possibility of high-performance, guidestar-free adaptive optics. Recently, Feng et al. [16] demonstrated that from a natural blurry image,

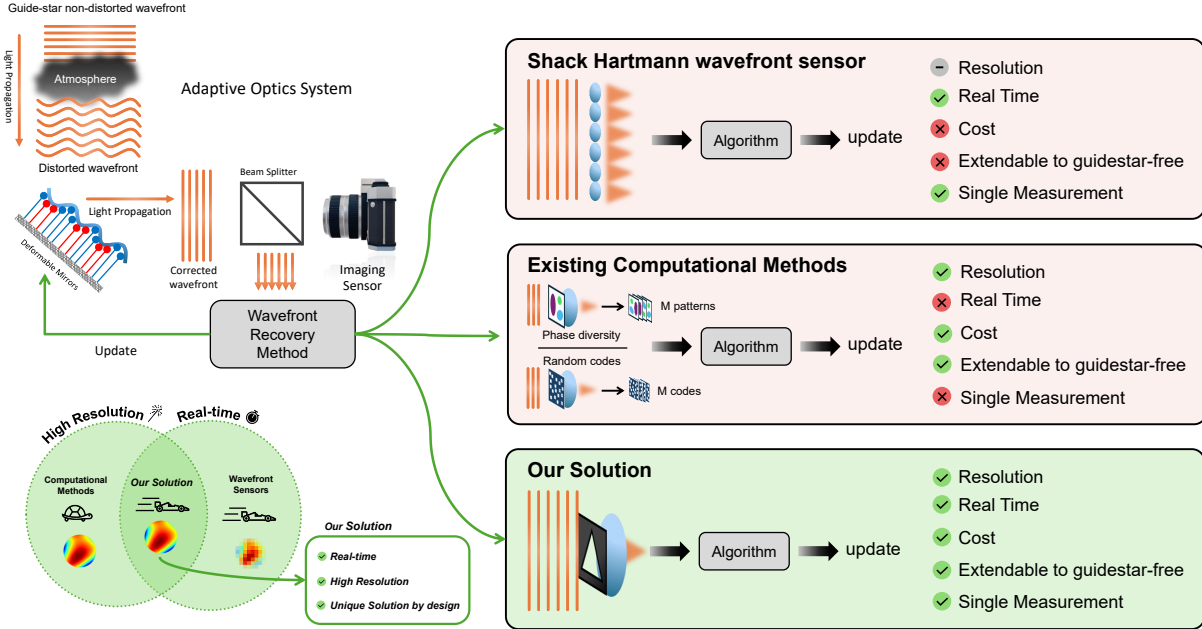


Fig. 1. Overview of adaptive optics (AO) and the position of our method among hardware and alternative computational methods for wavefront estimation.

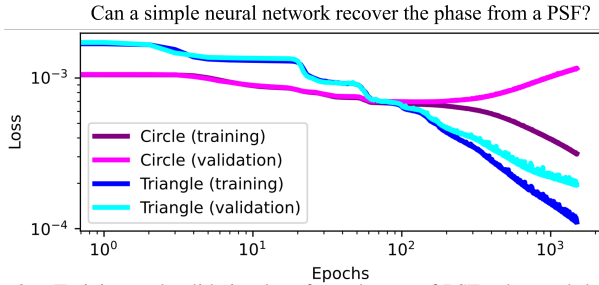


Fig. 2. Training and validation loss for a dataset of PSFs observed through circular and triangular pupils. Using a circular pupil causes overfitting while the triangular pupil allows reasonable generalization to validation data.

one can recover the PSF and corresponding wavefront with a compute time on the order of minutes. This paper offers the complementary capability of recovering the wavefront from a single PSF at thousands of frames per second. We provide an overview of this method in the context of alternatives in Figure 1.

### B. Preview of main results

A key observation we make in this paper is that most pupils are a circle — this is how we design our imaging systems. However, a circular pupil creates a critical issue in wavefront estimation: the support of its conjugate-flip is identical. So, if we want to resolve trivial ambiguity, we need to *break the symmetry!* As we will show later in the paper, we can identify conditions under which there exist *invertible point spread functions (iPSFs)* such that the phase can be recovered suitably for adaptive optics.

To convince readers of the significance of pupil geometry, in Figure 2 we show the training and validation performance for recovering phase uniquely from a Fourier magnitude. The “algorithm” we use to perform the phase recovery task

is to train a simple multi-layer perceptron (MLP); we are not advocating in favor of a learning-based solution over other well-established convex optimization algorithms, we are merely illustrating the importance of geometry. The training and validation curves in Figure 2 show a clear contrast between the two geometries. For the circular aperture, even if we can drive the training loss down, the validation loss will increase, implying that the network cannot generalize. The triangle aperture has a much better behavior as far as training and validation are concerned. As we shall explain more precisely later, this is not a failure of network design – it is explainable from the types of ambiguities permitted by the two geometries.

We outline the contributions of this paper as follows:

- 1) **Practical conditions for invertible PSFs.** We prove there exists a set of practically achievable conditions for wavefront estimation from an incoherent PSF in which the solution is unique. Therefore, one can build an imaging system whose phase can be uniquely determined. We refer to these as invertible PSFs.
- 2) **Unique wavefront estimation algorithms using a single PSF.** We describe and compare a few varieties of networks that can perform real-time PSF inversion, operating near or faster than consumer-grade high-speed Shack-Hartmann sensors and offering high accuracy for downstream adaptive optics correction.

## II. BACKGROUND AND PHASE RETRIEVAL

### A. Notation

In this paper, we focus on 2D problems, though it can be generalized to  $d$  dimensions [6], [8], [17]. A 2D complex signal is denoted as  $x[\mathbf{n}] \in \mathbb{C}$ , where  $\mathbf{n} = (n_1, n_2)$  denotes the spatial index. Without loss of generality, we assume  $\mathbf{n}$  is defined on a regular grid so that  $n_i \in \{0, \dots, N_i - 1\}$  where

$N_i$  is the number of points along each dimension of the grid  $\mathbb{Z}_N = \{0, \dots, N_1 - 1\} \times \{0, \dots, N_2 - 1\}$ .

The signal  $x[\mathbf{n}]$  contains magnitude and phase  $\phi[\mathbf{n}] \in \mathbb{R}$ ,

$$x[\mathbf{n}] = |x[\mathbf{n}]| e^{j\phi[\mathbf{n}]}. \quad (2)$$

We use  $\mathbf{x} \in \mathbb{C}^N$  to denote an  $N$ -dimensional vector  $\mathbf{x} = [x[\mathbf{n}_1], \dots, x[\mathbf{n}_N]]^T$ . For a 2D regular grid, it is easy to see that  $N = N_1 N_2$ . To specify the vector of the magnitude of  $\mathbf{x}$ , we write  $|\mathbf{x}| = [|x[\mathbf{n}_1]|, \dots, |x[\mathbf{n}_N]|]^T$ . Similarly, for the phase, we write  $\phi = [\phi[\mathbf{n}_1], \dots, \phi[\mathbf{n}_N]]^T$ .

We define the discrete Fourier transform (DFT) as

$$y[\mathbf{m}] = \frac{1}{M} \sum_{\mathbf{n} \in \mathbb{Z}_N} x[\mathbf{n}] e^{-j2\pi \mathbf{m}^T \mathbf{n} / M}, \quad (3)$$

where  $\mathbf{m} = (m_1, m_2)$  is the output coordinate with  $m_i = 0, \dots, M_i - 1$ , and  $M = M_1 M_2$ . The output vector is defined as  $\mathbf{y} = [y[\mathbf{m}_1], \dots, y[\mathbf{m}_M]]^T$ .

For a typical DFT, the input dimension  $N_i$  and output dimension  $M_i$  satisfy  $M_i = N_i$ . However, in phase retrieval, we often need to *oversample* in the output space. In this case, we will have  $M_i \geq N_i$ , corresponding to padding  $M_i - N_i$  zeros to each dimension of the input  $x[\mathbf{n}]$  before performing the DFT. Assuming that the oversampling is equal across all dimensions, we define the oversampling ratio as  $s \stackrel{\text{def}}{=} M/N$ . For notational convenience, we also define the oversampled Fourier transform matrix  $\mathbf{F} \in \mathbb{C}^{M \times N}$  with  $M \geq N$ . Therefore,  $\mathbf{y} = \mathbf{F}\mathbf{x}$  represents a  $M \times N$  discrete Fourier transform on a zero-padded input  $x[\mathbf{n}]$ .

### B. Phase retrieval and trivial ambiguities

**Definition 1** (Phase Retrieval). *Let  $\mathbf{x} \in \mathbb{C}^N$  be the ground truth complex signal, and let  $\mathbf{y} = |\mathbf{F}\mathbf{x}|^2 \in \mathbb{R}^M$  be the Fourier magnitude-square where  $\mathbf{F} \in \mathbb{C}^{M \times N}$  is the oversampled DFT matrix. The phase retrieval problem is defined as*

$$\text{Find } \hat{\mathbf{x}} \quad \text{such that} \quad \mathbf{y} = |\mathbf{F}\hat{\mathbf{x}}|^2. \quad (4)$$

In this paper, we are interested in the following three types of solutions that can be derived from the true signal  $\mathbf{x}$ .

**Definition 2.** *Let  $x[\mathbf{n}]$  be the ground truth signal. We define DC phase offset, translation<sup>1</sup>, and conjugate flip as follows.*

$$\begin{aligned} \mathcal{T}_{dc}\{\mathbf{x}\}[\mathbf{n}] &= x[\mathbf{n}] e^{j\phi_0}, & \text{for any } \phi_0 \in [0, 2\pi), \\ \mathcal{T}_{shift}\{\mathbf{x}\}[\mathbf{n}] &= x[\mathbf{n} - \ell], & \text{for any } \ell \in \mathbb{Z}_N, \\ \mathcal{T}_{flip}\{\mathbf{x}\}[\mathbf{n}] &= x^*[-\mathbf{n}]. \end{aligned}$$

*These operations can be defined elementwise for any vector  $\mathbf{x}$ , thus giving us  $\mathcal{T}_{dc}(\mathbf{x})$ ,  $\mathcal{T}_{shift}(\mathbf{x})$ ,  $\mathcal{T}_{flip}(\mathbf{x})$ , respectively.*

**Definition 3** (Trivial Ambiguity). *Given a vector  $\mathbf{x}$ , the trivial ambiguity set  $\Omega(\mathbf{x})$  contains all vectors generated by*

$$\Omega(\mathbf{x}) = \{\{\mathcal{T}_{dc}(\mathbf{x}), \mathcal{T}_{shift}(\mathbf{x}), \mathcal{T}_{flip}(\mathbf{x})\}\}, \quad (5)$$

*where  $\{\{\}\}$  denotes closure of the set under compositions.*

<sup>1</sup>The translation here is a circular translation. This ensures consistency when we perform Fourier analysis. Thus, strictly speaking, we should write  $\mathcal{T}_{shift}\{x[\mathbf{n}]\} = x[\mathbf{n} - \ell \bmod N]$ . But given this cumbersome notation, we write  $x[\mathbf{n} - \ell]$  with the implied meaning of circular wrapping.

**Property 1** (Bendory et al. [6]). *Let  $\mathbf{x} \in \mathbb{C}^N$  be a complex vector and  $\mathbf{F} \in \mathbb{C}^{M \times N}$  be the Fourier transform matrix. Then, any trivial ambiguity will give us the same Fourier magnitude:*

$$\hat{\mathbf{x}} \in \Omega(\mathbf{x}) \implies |\mathbf{F}\hat{\mathbf{x}}|^2 = |\mathbf{F}\mathbf{x}|^2. \quad (6)$$

In addition to trivial ambiguities, there also exist non-trivial ambiguities such that  $\hat{\mathbf{x}} \notin \Omega(\mathbf{x})$  but  $|\mathbf{F}\hat{\mathbf{x}}|^2 = |\mathbf{F}\mathbf{x}|^2$ . Non-trivial ambiguities are of significant importance in the literature as they correspond to signals with an entirely different structure than what  $\mathbf{x}$  actually represents.

### C. Known results about uniqueness

In the phase retrieval literature, an algorithm declares success if the only ambiguities its solution encounters are the trivial ambiguities [18], [19]. Most of the known uniqueness results are the non-trivial ones. These non-trivial solutions are plenty for 1D problems, e.g., Hassibi and collaborators [5] mentioned that there are up to  $2^N$  of them where  $N$  is the number of variables (i.e., pixels) for the phase.

Overcoming the non-trivial ambiguities is usually centered around two themes: oversampling rate and prior information (e.g., sparsity) [5]. The minimum oversampling rate is  $M \geq 2N$  if the sampling matrix is the DFT matrix. For a general sampling matrix, the consensus is  $M \geq 4N - 4$  [7] which is called the “ $(4N - 4)$  conjecture” [20] and is proven in [21]. For sparsity, various papers have demonstrated different degrees of uniqueness based on the periodicity of the signal and other properties of the signal (e.g., collision-free in [8]). There is also interest in probabilistic analysis of the uniqueness of a random measurement matrix [5], [11], [22].

The good news about non-trivial ambiguities is that although they play a big role in 1D phase retrieval, they have negligible effects in 2D. The following theorem from Hayes shows that the set of non-trivial ambiguities is measure zero.

**Theorem 1** (Hayes’ Theorem [17], [23]: Non-trivial Ambiguities have measure zero in 2D). *Let  $\mathbf{x} \in \mathbb{C}^N$  be the ground truth, and define  $\mathbf{y} = |\mathbf{F}\mathbf{x}|^2 \in \mathbb{R}^M$  be the Fourier magnitude-square. If  $d \geq 2$  and if the oversampling ratio is  $s = M/N \geq 2$  (i.e., at least twice the Nyquist rate per dimension), then it is almost surely (a.s.) that there does not exist a non-trivial solution  $\hat{\mathbf{x}}$  with  $\mathbf{y} = |\mathbf{F}\hat{\mathbf{x}}|^2$  and  $\hat{\mathbf{x}} \notin \Omega(\mathbf{x})$ .*

*Proof.* See [6], [17], [23]. □

### D. Fourier phase retrieval methods

Assuming Hayes’ result applies, much of the prior research then focuses on how to obtain the solution efficiently and robustly (against noise). Earlier approaches mostly follow the Gerchberg-Saxton algorithm [3] where the solution is obtained by alternately projecting the estimate onto a subspace in the time domain and constraining the Fourier magnitude. Follow-up works of Fienup [4], [24]–[27] introduced additional spatial restrictions and projections. The Hybrid Input-Output (HIO) algorithm by Fienup is still a popular algorithm today, even though the algorithm is not guaranteed to converge, and when it converges, it is not necessarily a global minimum.

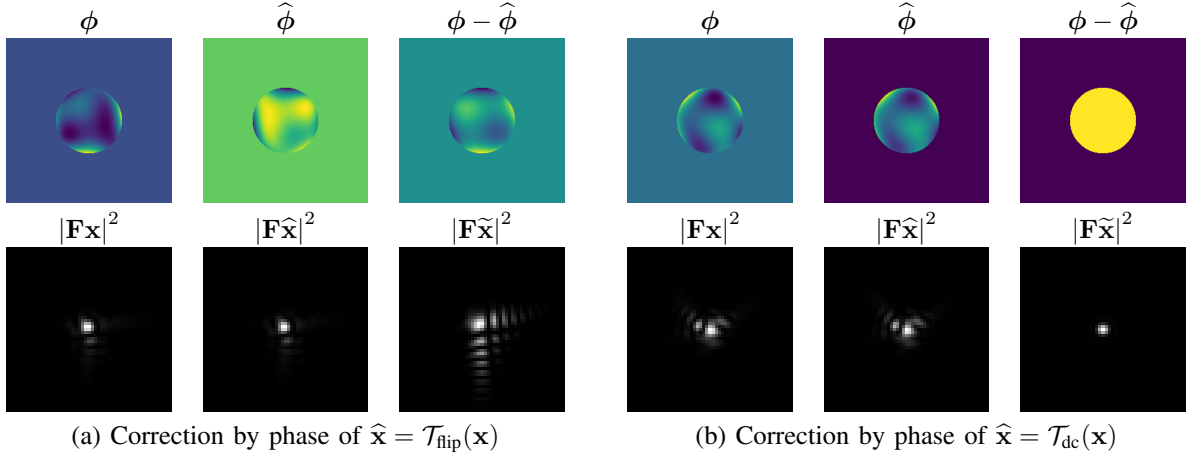


Fig. 3. Comparing the equivalence classes of phase retrieval and wavefront estimation. Phase aberrations [Top] are shown with their resulting PSFs [Bottom] with  $\mathbf{y} = |\mathbf{F}\mathbf{x}|^2$  where  $\mathbf{y}$  is the PSF and  $\phi$  is the phase of  $\mathbf{x}$ . In (a) we can see the PSFs match, though the optical correction does not achieve near-diffraction-limit performance. In (b) the PSFs also match, but  $\phi$  and  $\phi'$  only differ by an additive constant over the support. Thus, the optical correction achieves diffraction-limited performance.

Beyond Gerchberg-Saxton and Fienup which belong to the category of projection algorithms [28]–[30], there are other directions including gradient-based methods [31]–[33], convex relations methods which lift the phase retrieval to a matrix completion problem [34]–[38], spectral methods to initialize the estimation [32], [39]–[41], and Bayesian methods such as approximate message passing [42] and belief-propagation [43].

#### E. Other known techniques

**Coded Imaging.** A significant amount of the literature uses multiple *coded* measurements pioneered by Candès [34] and other researchers [36]–[38]. Coded sampling can be achieved in various ways such as (i) masking [44], [45], (ii) optical grating [46], [47], (iii) oblique illumination [48]. During the sensing process, the coding scheme (e.g., the mask) is shuffled to ensure a certain degree of de-correlation across the *multiple* measurements. This will then allow the reconstruction algorithm to achieve a globally unique solution. For us, since we are interested in real-time applications, we aim to perform wavefront estimation using a single measurement.

**Neural Wavefront Sensing.** A relatively new approach is neural wavefront shaping by Feng. et al. [16] where the wavefront signal is encoded by a neural radiance field. By jointly optimizing the reconstruction neural network and the phase mask, wavefront estimation can be achieved. Neural wavefront shaping relies on redundant measurements; it is reported in [49] that they need at least 16 different spatial light modulator (SLM) patterns (often tens to hundreds).

**Deep Learning.** Deep learning approaches are plentiful. But if we closely inspect these methods, they are conceptually very similar to traditional methods, except that some steps are implemented through neural networks. For example, when solving the optimization, instead of resorting to classical methods such as ADMM, one can use Plug-and-Play [50] by integrating pre-trained image denoisers to improve the prior. If we want more explicit control over the prior, generative priors can be used [51], [52]. One can also replace the entire optimization-based approach with an end-to-end neural

network, such as [53], [54]. A recent tutorial, Lam et al. [55], has an excellent taxonomy of deep learning methods for phase retrieval to which we refer interested readers.

### III. UNIQUENESS OF WAVEFRONT ESTIMATION

#### A. What is wavefront estimation?

To motivate the wavefront estimation problem, we need to briefly describe how adaptive optics work. When an image is formed by an optical system, the response of the system is described by its point spread function (PSF). The PSF is said to be at the diffraction limit when it is free of aberrations. Aberrations are introduced when imaging through random media or in the presence of sub-optimal optical components.

The goal of adaptive optics is to compensate for these aberrations in real-time. Let  $\phi[\mathbf{n}]$  be the ground truth and  $\hat{\phi}[\mathbf{n}]$  be the estimate. The mathematical operation of this compensation is then as follows:

$$\underbrace{\tilde{x}[\mathbf{n}]}_{\text{compensated signal}} \stackrel{\text{def}}{=} \underbrace{|x[\mathbf{n}]|e^{j\phi[\mathbf{n}]}}_{\text{original } x[\mathbf{n}]} \times \underbrace{e^{-j\hat{\phi}[\mathbf{n}]}}_{\text{compensation}}. \quad (7)$$

The quality of this operation is then determined by the resulting PSF, i.e.,  $|\mathbf{F}\tilde{\mathbf{x}}|^2$ . If  $|\mathbf{F}\tilde{\mathbf{x}}|^2$  is a diffraction-limited spot, then the compensation can be declared a success.

**Example 1.** [Conjugate Flip] Consider a ground truth phase  $\phi[\mathbf{n}]$  and the corresponding signal  $x[\mathbf{n}] = |x[\mathbf{n}]|e^{j\phi[\mathbf{n}]}$ . We apply a conjugate flip trivial ambiguity to  $x[\mathbf{n}]$  by considering  $\hat{\phi}[\mathbf{n}] = -\phi[-\mathbf{n}]$  so that  $\hat{x}[\mathbf{n}] = x[\mathbf{n}]e^{j\hat{\phi}[\mathbf{n}]} = \mathcal{T}_{\text{flip}}(x[\mathbf{n}]) = x^*[-\mathbf{n}]$ . It is easy to show that  $|\mathbf{F}\mathbf{x}| = |\mathbf{F}\hat{\mathbf{x}}|$ . An adaptive optics system that uses this  $\hat{\phi}$  to compensate for the phase  $\phi$  producing  $\phi - \hat{\phi}$  is shown in Figure 3(a). If we take the corresponding Fourier magnitude square of the compensated signal, we will see a worsened PSF.

**Example 2.** [DC Offset] Consider a ground truth phase  $\phi[\mathbf{n}]$  and the corresponding signal  $x[\mathbf{n}] = |x[\mathbf{n}]|e^{j\phi[\mathbf{n}]}$ . This time we consider a DC offset trivial ambiguity  $\hat{\phi}[\mathbf{n}] = \phi[\mathbf{n}] + \phi_0$  so that  $\hat{x}[\mathbf{n}] = x[\mathbf{n}]e^{j\hat{\phi}[\mathbf{n}]} = \mathcal{T}_{\text{dc}}(x[\mathbf{n}]) = x[\mathbf{n}]e^{j\phi_0}$ . We can again show that  $|\mathbf{F}\mathbf{x}| = |\mathbf{F}\hat{\mathbf{x}}|$ . Using an adaptive optics correction

with this  $\hat{\phi}$  results in a phase profile as shown in Figure 3(b). If we take the corresponding Fourier magnitude square of the compensated signal, we will see a diffraction-limited spot.

In summary, the conjugate flip degrades our system while a DC offset is immaterial. This leads to the question: How do we check whether a candidate solution  $\hat{\mathbf{x}}$  is worsening the imaging system? One way to do this is to consider a criterion:

$$\underbrace{\sum_{\mathbf{n}} |x[\mathbf{n}]|^2}_{|\mathbf{x}^H \mathbf{x}|, \text{ ideal PSF}} \stackrel{?}{=} \underbrace{\sum_{\mathbf{n}} |x[\mathbf{n}]|^2 e^{j(\phi[\mathbf{n}] - \hat{\phi}[\mathbf{n}])}}_{\mathbf{x}^H \hat{\mathbf{x}}, \text{ compensated PSF}} \quad (8)$$

This equation checks whether the complex conjugate  $\mathbf{x}^H$  is “aligned” with the estimated phase  $\hat{\mathbf{x}}$ . If it does, then the product will give us the magnitude square of the signal. It is easy to show that the conjugate flip does not satisfy this criterion whereas the DC offset does.

Based on the intuition given in (8), we define the wavefront estimation problem as follows:

**Definition 4** (Wavefront Estimation). *Let  $\mathbf{x} \in \mathbb{C}^N$  be the ground truth complex signal, and define  $\mathbf{y} = |\mathbf{F}\mathbf{x}|^2 \in \mathbb{R}^M$  be the Fourier magnitude. We define the wavefront estimation problem as*

$$\text{Find } \hat{\mathbf{x}} \text{ such that } \mathbf{y} = |\mathbf{F}\hat{\mathbf{x}}|^2 \text{ and } |\mathbf{x}^H \hat{\mathbf{x}}| = |\mathbf{x}^H \mathbf{x}|. \quad (9)$$

We call  $|\mathbf{x}^H \hat{\mathbf{x}}| = |\mathbf{x}^H \mathbf{x}|$  the **optical correction constraint**.

Comparing (9) and (4), we recognize that while both phase retrieval and wavefront estimation aim to recover the phase from Fourier magnitude, wavefront estimation requires an optical correction constraint to reject trivial ambiguities. Therefore, wavefront estimation is a sub-problem of phase retrieval.

### B. Geometry of pupil

The shape of the pupil plays a big role in wavefront estimation. We define the pupil function below.

**Definition 5** (Pupil). *The pupil  $\mathbf{p} \in \mathbb{R}^N$  is an indicator function defined such that*

$$p[\mathbf{n}] = \begin{cases} 1 & |x[\mathbf{n}]| \neq 0 \\ 0 & |x[\mathbf{n}]| = 0 \end{cases}, \quad \forall \mathbf{n} \in \mathbb{Z}_N. \quad (10)$$

Therefore, the vector  $\mathbf{p}$  denotes a binary mask. In the absence of any phase aberration, i.e.,  $\phi[\mathbf{n}] \equiv 0$  for all  $\mathbf{n}$ , the shape of the pupil will determine the diffraction-limited spot.

**Definition 6** (Diffraction limited PSF). *Let  $\mathbf{x} \in \mathbb{C}^N$  and  $x[\mathbf{n}] = p[\mathbf{n}]e^{j\phi[\mathbf{n}]}$  be the system response, i.e., the magnitude is  $|\mathbf{x}| = \mathbf{p}$ . If  $\phi[\mathbf{n}] \equiv 0$  for all  $\mathbf{n}$ , then the PSF given by*

$$\mathbf{y} = |\mathbf{F}\mathbf{p}|^2 \quad (11)$$

is called a **diffraction-limited PSF**.

The diffraction-limited PSF provides us with a convenient way to measure the quality of the estimated wavefront. In the optics literature, the most commonly used metric is known as the Strehl ratio [1].

**Definition 7** (Strehl Ratio). *Let  $\hat{\mathbf{x}}$  be the estimated optical aberration. We define the Strehl ratio as*

$$q \stackrel{\text{def}}{=} \max \left\{ |\mathbf{F}\hat{\mathbf{x}}|^2 \right\} / \max \left\{ |\mathbf{F}\mathbf{p}|^2 \right\}. \quad (12)$$

where  $q$  is a number between  $0 \leq q \leq 1$ .

A Strehl ratio of  $q = 1$  corresponds to a diffraction limited PSF while a Strehl ratio  $q \ll 1$  is a severely distorted PSF.

### C. Main result 1: Impact of the constraint

We now present our first main result regarding the wavefront estimation problem formulation (9). We show that while there are many trivial ambiguities of the original phase retrieval problem in (4), by adding the optical correction constraint in (9) the set of solutions reduces to complex scalar multiples of the true solution.

**Theorem 2.** *Let  $\mathbf{x} \in \mathbb{C}^N$  be the ground truth complex signal, and let  $\hat{\mathbf{x}} \in \Omega(\mathbf{x})$  be one of the trivial solutions obtained by solving the original phase retrieval (4). If  $\hat{\mathbf{x}}$  satisfies the optical correction constraint  $|\mathbf{x}^H \hat{\mathbf{x}}| = |\mathbf{x}^H \mathbf{x}|$  defined in (9), then it is necessary that*

$$\hat{x}[\mathbf{n}] = x[\mathbf{n}]e^{jc}, \quad (13)$$

for some  $c \in [0, 2\pi)$ .

*Proof.* See Appendix.  $\square$

The following two Corollaries discuss the impact of using solutions to (9) in the context of phase conjugate AO.

**Corollary 1.** *Let  $\mathbf{x} \in \mathbb{C}^N$  be the ground truth complex signal, and let  $\hat{\mathbf{x}} \in \Omega(\mathbf{x})$  be the solution of (9). Then, if we compensate  $\mathbf{x}$  by multiplying the phase component of  $\hat{\mathbf{x}}$ , the compensated signal is*

$$\tilde{x}[\mathbf{n}] = |x[\mathbf{n}]|e^{j\phi[\mathbf{n}]} \times e^{-j\hat{\phi}[\mathbf{n}]} = |x[\mathbf{n}]|e^{-jc},$$

for some  $c \in [0, 2\pi)$ .

*Proof.* Theorem 2 implies that  $\hat{x}[\mathbf{n}] = x[\mathbf{n}]e^{jc}$ , which gives us  $\hat{\phi}[\mathbf{n}] = \phi[\mathbf{n}] + c$  for  $c \in [0, 2\pi)$ . Thus  $\forall \mathbf{n} \in \mathbb{Z}_N$ ,

$$\begin{aligned} \tilde{x}[\mathbf{n}] &\stackrel{\text{def}}{=} |x[\mathbf{n}]|e^{j\phi[\mathbf{n}]} \times e^{-j\hat{\phi}[\mathbf{n}]} \\ &= |x[\mathbf{n}]|e^{j(\phi[\mathbf{n}] - \phi[\mathbf{n}] - c)} = |x[\mathbf{n}]|e^{-jc}. \end{aligned}$$

$\square$

In the special case where the magnitude of  $\mathbf{x}$  is just the pupil function, i.e.,  $\mathbf{x} = \mathbf{p}e^{j\phi}$ , the solution of (9) will give us the ideal Strehl ratio of  $q = 1$  as summarized in Corollary 2.

**Corollary 2.** *Let  $\mathbf{x} \in \mathbb{C}^N$  be the ground truth complex signal, and suppose that  $x[\mathbf{n}] = p[\mathbf{n}]e^{j\phi[\mathbf{n}]}$ . Let  $\hat{\mathbf{x}} \in \Omega(\mathbf{x})$  be the solution of (9). Then, the phase compensated signal  $\tilde{\mathbf{x}}$  will have a Strehl ratio of  $q = 1$ .*

*Proof.* Corollary 1 implies that  $\tilde{\mathbf{x}} = |\mathbf{x}|e^{-jc}$ . Since  $|\mathbf{x}| = \mathbf{p}$ , we have  $\tilde{\mathbf{x}} = \mathbf{p}e^{-jc}$  for  $c \in [0, 2\pi)$ . Thus, by definition of

the Strehl ratio, the phase compensated signal  $\tilde{\mathbf{x}}$  will have a Strehl ratio of

$$\begin{aligned} q &= \max \left\{ |\mathbf{F}\tilde{\mathbf{x}}|^2 \right\} / \max \left\{ |\mathbf{F}\mathbf{p}|^2 \right\} \\ &= \max \left\{ |e^{-j\mathbf{c}}\mathbf{F}\mathbf{p}|^2 \right\} / \max \left\{ |\mathbf{F}\mathbf{p}|^2 \right\} = 1, \end{aligned}$$

since  $e^{-j\mathbf{c}}$  can be eliminated.  $\square$

These results indicate that if we can find a solution to (9), we will recover the solution  $\mathbf{x}$  up to a DC shift, i.e., a multiplication with a complex exponential. Furthermore, if we can recover  $\mathbf{x}$  up to this set, the resulting phase conjugation can be said to be optimal.

#### D. Main result 2: invertible PSF

Hayes' Theorem and Theorem 2 have little to do with the ease of recovery because one cannot resolve the trivial ambiguities. We now turn towards defining an invertible PSF and presenting the second key Theorem of this paper. We derive a set of conditions under which a PSF is invertible. The implication of these constraints is a set of *imaging systems* that produce *only* PSFs whose phase can be uniquely estimated.

**Definition 8** (Invertible PSF). *Let  $\mathbf{x} \in \mathbb{C}^N$  and  $x[\mathbf{n}] = p[\mathbf{n}]e^{j\phi[\mathbf{n}]}$  with  $\mathbf{n} \in \mathbb{Z}_N$ . If for every  $\hat{\mathbf{x}} \neq \mathbf{x}$  that satisfies  $|\mathbf{F}\hat{\mathbf{x}}| = |\mathbf{F}\mathbf{x}|$  the optical correction constraint  $|\mathbf{x}^H\hat{\mathbf{x}}| = |\mathbf{x}^H\mathbf{x}|$  is also satisfied, then we say  $\mathbf{y} = |\mathbf{F}\mathbf{x}|^2$  is an invertible PSF.*

The following Theorem describes how to design a system that produces only invertible PSFs.

**Theorem 3** (Existence of invertible PSF imaging system). *Let  $|x[\mathbf{n}]| > 0$  for some subset of  $\mathbb{Z}_N$ . Suppose that the measurement  $y[\mathbf{m}]$  with  $d \geq 2$  is oversampled by a factor  $s \geq 2$  under measurement model (3). The set of trivial ambiguities  $\Omega(\mathbf{x})$  is reduced to the unique solution  $\{\mathbf{x}\}$  (a.s.) if all of the following conditions are met:*

- (i) *The pupil  $p[\mathbf{n}]$  is known a priori  $\forall \mathbf{n} \in \mathbb{Z}$ ;*
- (ii) *The shifted pupil is aperiodic:  $\mathcal{T}_{\text{shift}}(\mathbf{p}) \neq \mathbf{p}$  for any amount of non-zero (circular) shift;*
- (iii) *The flipped pupil is aperiodic:  $\mathcal{T}_{\text{shift}} \circ \mathcal{T}_{\text{flip}}(\mathbf{p}) \neq \mathbf{p}$  for any amount of (circular) shift;*
- (iv) *The average value of the phase offset by  $\mathcal{T}_{dc}$  is known.*

*Proof.* See Appendix.  $\square$

Under the above conditions, the corresponding phase retrieval has *only* one solution, i.e.,  $\hat{\mathbf{x}} = \mathbf{x}$ , almost surely (a.s.). Furthermore, with the exception of  $\mathbf{x} \neq \mathbf{0}$  and condition (iv), the constraints are all on the *geometry* of the pupil  $\mathbf{p}$  which, in the context of optics, can be *designed*.

**Understanding the Geometry.** Among the four conditions above, the most interesting ones are (ii) and (iii). We use Figure 4 to illustrate the idea. The first support shown satisfies all conditions, the second does not satisfy condition (ii), and the final two do not satisfy condition (iii).

**Toy Example.** We use an example to highlight the impact of our conditions on the inverse problem (9). Consider a phase that is the sum of two astigmatism Zernike polynomials,  $\phi[\mathbf{n}] = a_5 Z_5[\mathbf{n}] + a_6 Z_6[\mathbf{n}]$ , with ground truth  $a_5 = a_6 = 2$  and

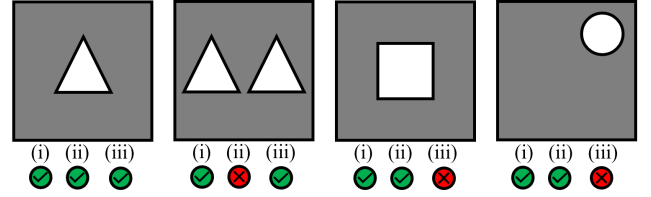


Fig. 4. Visualizing various pupil geometries that do and do not satisfy pupil geometry conditions (i-iii) of Theorem 3.

$Z_\ell[\mathbf{n}]$  is the  $\mathbf{n}$ th sample of the  $\ell$ th Zernike polynomials [56], [57]. We construct the signal as  $x[\mathbf{n}] = p[\mathbf{n}]e^{j\phi[\mathbf{n}]}$ . Given the Fourier magnitude  $\mathbf{y} = |\mathbf{F}\mathbf{x}|^2$ , we want to recover  $(a_5, a_6)$ .

We consider four different pupil shapes as shown in Figure 5. The shapes of the pupils are known a priori, and they will replace  $p[\mathbf{n}]$  when defining  $x[\mathbf{n}]$ . We are interested in (i) finding the phase retrieval solution by solving the original problem (4) using different shapes; and (ii) inspecting the optimization landscape, i.e., the objective function.

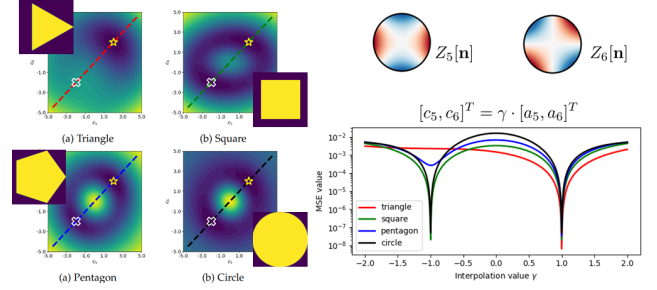


Fig. 5. Toy example illustrating the impact of pupil geometry on recovery.

Figure 5(a)-(d) shows the objective function which is a 2D function of variables  $(a_5, a_6)$ . The true solution is  $(a_5, a_6) = (2, 2)$  (marked as a star), and the conjugate flip is  $(a_5, a_6) = (-2, -2)$ . We cut the cross section along the diagonal, and we plot the energy level on the right-hand side of Figure 5. To make our plots consistent across the four cases, we use a dummy parameter  $\gamma$  to control the sweep between solutions and plot along  $\gamma(a_5, a_6)$ , hence  $\gamma = 1$  is the true solution case and  $\gamma = -1$  is the conjugate flip case.

Based on the plot, we can make the following observations:

- **Circle:** There are two equally good global minima, no matter what algorithm we use there is a 50% chance we will hit the correct solution and a 50% chance the conjugate flip. We cannot distinguish the two.
- **Square:** The behavior is very similar to a circle where there are two equally good global minima. Again, we cannot distinguish the two.
- **Triangle:** There is only one local minimum, and this local minimum *is* the correct solution.
- **Pentagon:** While we can see two local minima, their objective values are different. This implies that as long as we have a reasonably designed algorithm that can search for a better local minimum, we will get a unique solution.

In summary, if we use a non-centrosymmetric pupil (such as a triangle or a pentagon), we can identify the correct solution.

### E. Hasn't symmetry breaking been used for a long time?

In optics, symmetry breaking has been reported by Fienup [18], [19], [24], [58], [59] in the 1980's. The difference is that in Fienup's work, the approach is largely about finding the appropriate boundary conditions of the autocorrelation function [60]. Because the approach boils down to solving a system of linear equations, it is unclear how one can readily generalize the concept to analyze the optimal geometry or design neural networks. Other works such as [61] and [62] have specific choices of the aperture but they are limited to highly customized problems.

In signal processing, interestingly, there are limited discussions about symmetry breaking. The most relevant comments were made by Sun and collaborators [63], [64] where they observed the same phenomenon we present here, but their approach introduces constraints in the training dataset. For us, instead of manipulating the data we re-design the optics.

### F. Going from uniqueness in $\mathbf{x}$ to $\phi$

Up to this point, we have considered the recovery of  $\mathbf{x} \in \mathbb{C}^N$ , though we are often more interested in finding  $\phi \in \mathbb{R}^N$ . However, the uniqueness in  $\mathbf{x}$  does not guarantee uniqueness in  $\phi$ . To achieve uniqueness in  $\phi$  by uniqueness in  $\mathbf{x}$ , we must meet two (additional) requirements related to phase unwrapping:

- 1) The difference between neighboring samples of  $\phi[\mathbf{n}]$  can not exceed  $\pm\pi$ , thus the phase can be recovered up to an average value by phase unwrapping. One can interpret this as a smoothness constraint.
- 2) The average value of  $\phi[\mathbf{n}]$  is 0, i.e.,  $\mathbf{p}^T \phi = 0$ . Note we have already assumed this WLOG previously.

Under these two conditions, the uniqueness in  $\mathbf{x}$  (from Theorem 3) can be transferred to  $\phi$  which follows from the phase unwrapping problem being uniquely solvable [65].

## IV. WAVEFRONT ESTIMATION ALGORITHMS

Now that we understand how to design our pupil, the next big question is how to rapidly estimate the phase. In this section, we propose a few wavefront estimation algorithms for non-circular apertures. We additionally describe the use of neural representations to calibrate for the shape.

### A. Proposed methods for phase recovery

In developing a wavefront estimation algorithm, uniqueness provides a significant benefit. If the problem has a unique solution, a network can be trained in a supervised fashion to invert PSFs. On the other hand, if an imaging system does not have an invertible PSF, then the network will not generalize as shown in Figure 2.

In what follows, we present a few *efficient* algorithms that can invert PSFs in real time. Our algorithms are inspired by previous methods in the literature. We do not necessarily advocate for one method over another. Our goal here is to demonstrate that if the solution is unique then one has a lot of flexibility in designing the network. We consider three classes of algorithms: (i) direct methods, (ii) unrolled methods and (iii) neural representations.

1) *Proposed method 1 (inspired by [66]): Direct PSF inversion:* A PSF is band-limited by definition. Because of this, we consider writing a PSF as a linear combination of basis functions:

$$y[\mathbf{n}] = \sum_{k=1}^K \beta_k \zeta_k[\mathbf{n}], \quad (14)$$

where  $\beta_k \in \mathbb{R}$  is the  $k$ th basis coefficient and  $\zeta_k[\mathbf{n}]$  is the corresponding basis function, which can be obtained offline using supervised learning [66]. For notational simplicity we write  $\beta = \{\beta_1, \dots, \beta_K\}$ . Similarly, we write  $\phi[\mathbf{n}]$  as

$$\phi[\mathbf{n}] = \sum_{\ell=1}^L \alpha_\ell \xi_\ell[\mathbf{n}], \quad (15)$$

where  $\xi_\ell[\mathbf{n}]$  is an orthogonal basis over  $\mathbf{p}$ , and  $\alpha = \{\alpha_1, \dots, \alpha_L\}$ . We choose  $\xi$  to be the Zernike polynomials when  $\mathbf{p}$  is a circle.

While  $\alpha \rightarrow \beta$  was previously considered in [66], known as the Phase-to-Space (P2S) transform for simulating imaging through turbulence for simulation [67], [68], wavefront estimation requires  $\beta \rightarrow \alpha$ . As discussed previously,  $\beta \rightarrow \alpha$  is unique if Theorem 3 is satisfied. We refer to  $\beta \rightarrow \alpha$  as the Space-to-Phase (S2P) transform, which we approximate with a learned representation,  $\text{S2P}_\theta(\beta) \approx \alpha$ , using a lightweight 3-layer perceptron (MLP) with ReLU activation functions. The S2P method is illustrated in Figure 6.

To successfully train the S2P, aside from satisfying Theorem 3, we also find using basis functions that are orthogonal over the designed pupil  $\mathbf{p}$  helps significantly. For flexibility, we mask the Zernike polynomials by  $\mathbf{p}$  then perform Gram-Schmidt orthogonalization. Figure 7 shows various  $\xi$  basis functions obtained as described.

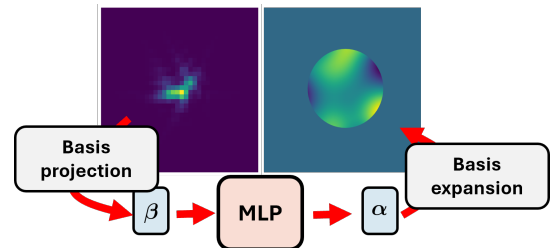


Fig. 6. The Space-to-Phase (S2P) transform overview.

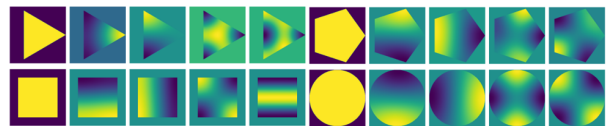


Fig. 7. Visualization of phase basis functions for different pupil geometries.

The S2P has a few advantages:

- (i) The S2P runs at  $\sim 5,200$  frames per second for a  $128 \times 128$  PSF on an AMD Ryzen 7 5700X3D CPU. This speed can be attributed to the usage of the basis representations, reducing the problem dimensionality.
- (ii) The S2P is robust to noise as high-frequency noise can not be captured in the low dimensional subspace spanned by the basis representation.

Aside from representing *both* the PSF and phase via basis representation, we additionally consider the mappings  $\mathbf{y} \rightarrow \boldsymbol{\alpha}$  and  $\mathbf{y} \rightarrow \phi$ . Surprisingly, we find the MLP structure described for the S2P works for these mappings as well, speaking to the well-posed nature of recovery given uniqueness.

2) *Proposed method 2 (inspired by [3], [4]): Unrolled PSF inversion:* Direct PSF inversion lacks a “feedback mechanism” such as those in the Gerchberg-Saxton [3] and HIO algorithm by Fienup [4]. An interesting quality of the HIO algorithm is the intuition that the intermediate “outputs” of the algorithm need not be the estimation of the measurement, but a driving function for the iterative algorithm. Following the HIO algorithm, we consider an unrolled version of the S2P in which the intermediate variables are not constrained to be wavefront estimations but simply driving functions for the final output. We summarize the unrolled S2P algorithm in Algorithm 1.

---

**Algorithm 1** Unrolled S2P network

---

**Require:** Input:  $\mathbf{y}$ ,  $\mathbf{p}$ , Output:  $\hat{\phi}$

```

 $\mathbf{y}_0 \stackrel{\text{def}}{=} \mathbf{y}$ 
for  $k = 1$  to  $K$  do
  if  $k = 1$  then
     $\boldsymbol{\alpha}_k \leftarrow g_{\theta_k}(\mathbf{y}_0)$ 
  else
     $\boldsymbol{\alpha}_k \leftarrow g'_{\theta_k}([\mathbf{y}_0, \mathbf{y}_{k-1}, \boldsymbol{\alpha}_{k-1}])$  //Concatenated inputs
  end if
   $\phi_k[\mathbf{n}] = \sum_{\ell} \alpha_{k,\ell} \xi_{\ell}[\mathbf{n}]$ 
   $\mathbf{y}_k \leftarrow |\mathbf{F}(\mathbf{p} \odot e^{j\phi_k})|^2$  //Can be accelerated via P2S
end for
return  $\hat{\phi} = \phi_K$ 

```

---

3) *Proposed method 3 (inspired by [16], [69]): Neural representation:* Using a basis representation in the phase retrieval problem was considered by Fienup [69]. Using this representation, one can perform gradient-based optimization on the following loss:

$$\hat{\boldsymbol{\alpha}} = \underset{\boldsymbol{\alpha}}{\operatorname{argmin}} \sum_{t=1}^T \left\| \mathbf{y}_t - \left| \mathbf{F} \left( \mathbf{p} \odot e^{j \sum_{\ell=1}^L \alpha_{\ell} \xi_{\ell}} \right) \right|^2 \right\|^2, \quad (16)$$

where  $\boldsymbol{\xi} = [\xi[\mathbf{n}_1], \dots, \xi[\mathbf{n}_N]]^T$  was chosen to be the Zernike polynomials in [69]. Recently, the Zernike polynomials were used as an encoding for implicit neural representations (INR) was proposed in [16] used to iteratively solve a modified version of (16). To fit our problem, we modify the Zernike encoding to be the  $\boldsymbol{\xi}$ -encodings shown in Figure 7. We refer to this as a  $\boldsymbol{\xi}$ -Encoded INR.

For Fienup [69], the Zernike representation reduced the dimensionality of the problem, offering some benefit over the standard GS and HIO algorithms, though the trade-off is that it relied on gradient-based methods making initialization crucial. The  $\boldsymbol{\xi}$ -encoded INR is a basis that is then passed through a non-linear transformation, hence it can be viewed as a generalization of a linear basis representation. We find that using the  $\boldsymbol{\xi}$ -encoded INR tends to perform well even in the presence of noise, likely due to the natural smoothness imposed by the INR. In the noiseless case, we will see the

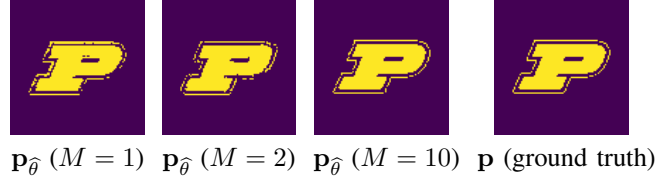


Fig. 8. Qualitative performance for pupil calibration problem. The subfigures above show the estimated pupil  $\mathbf{p}_{\hat{\theta}}$ . Here,  $M$  is the number of measurements.

that the  $\boldsymbol{\xi}$ -Encoded INR performs at or near the performance of the GS and HIO algorithms.

### B. Neural representations for pupil shape calibration

We now discuss the pupil calibration problem in which we no longer assume an exact knowledge of  $p[\mathbf{n}]$ . Suppose we can illuminate the pupil with a known signal with  $x[\mathbf{n}] = c[\mathbf{n}]e^{j\psi[\mathbf{n}]}$  where  $c[\mathbf{n}]$  is the support of the calibration pattern and  $\psi[\mathbf{n}]$  is the phase of the calibration pattern over  $c[\mathbf{n}]$  with the support of  $c[\mathbf{n}]$  beyond that of  $p[\mathbf{n}]$ . We define the following as the pupil identification problem:

**Definition 9** (Pupil Identification). *Given  $\psi$  and  $\mathbf{y}$ ,*

$$\text{Find } \mathbf{p} \text{ subject to } \mathbf{y} = |\mathbf{F}(\mathbf{p} \odot e^{j\psi})|^2, \quad (17)$$

where  $\odot$  represents the elementwise product of two vectors.

**Theorem 4** (Uniqueness of Pupil Shape Calibration). *Let calibration pattern  $\psi[\mathbf{n}]$  be known over support  $c[\mathbf{n}]$  and measurement  $\mathbf{y}[\mathbf{n}]$  satisfy Hayes’ Theorem. If there does not exist an  $\boldsymbol{\ell} \in \mathbb{Z}_N$  such that  $p[\pm\mathbf{n} + \boldsymbol{\ell}] \neq p[\mathbf{n}]$  and  $p[\pm\mathbf{n} + \boldsymbol{\ell}]e^{j\psi[\mathbf{n}]} \in \Omega(\mathbf{x})$  then the pupil shape  $p[\mathbf{n}]$  that satisfies (17) is unique (a.s.).*

*Proof.* See Appendix.  $\square$

This theorem can be stated intuitively: if there is no other way to position the pupil to produce the same PSF,  $p[\mathbf{n}]$  is unique. This imposes two requirements on  $\psi[\mathbf{n}]$  if we want to identify the pupil shape using a single measurement. The first requirement is that for a single calibration pattern,  $\psi[\mathbf{n}]$  can not be too “simple”. Second, it imposes a joint requirement on the shape of  $p[\mathbf{n}]$  and the chosen pattern  $\psi[\mathbf{n}]$ .

**Neural mapping implementation.** For optimizing the geometry of the pupil, we use a coordinate-encoded MLP with a standard positional Fourier encoding [70] to represent the pupil. Using a coordinate-encoded MLP is useful since the pupil is typically not a collection of delta functions, but some shape with a specific structure. Denoting

$$x_{\theta}^{(m)}[\mathbf{n}] = p_{\theta}[\mathbf{n}]e^{j\psi^{(m)}[\mathbf{n}]}, \quad (18)$$

where  $m$  indicates the corresponding measurement, the MLP aims to solve (17) via  $\ell^2$  loss. The final  $\mathbf{p}_{\hat{\theta}}$  is thresholded to give an estimate of the pupil. We display a qualitative result for pupil recovery in Figure 8 where our goal is to recover  $\mathbf{p}$  from  $M = \{1, 2, 10\}$  measurements.

TABLE I

PERFORMANCE ON PHASE RETRIEVAL AND WAVEFRONT ESTIMATION PROBLEMS FOR VARIOUS SUPPORT SHAPES WITH AND WITHOUT NOISE, WITH SPEED COMPARISONS. THE BEST AND SECOND-BEST PERFORMING ALGORITHMS ARE INDICATED WITH CELL SHADING AND UNDERLINED, RESPECTIVELY. ALGORITHMS PROPOSED IN THIS PAPER ARE INDICATED WITH A †.

Task: Phase retrieval (trivial ambiguities do not matter). Metric: Normalized correlation.								
Support	Condition	Iterative methods			S2P <sup>†</sup>	Direct methods		Other Unrolled S2P <sup>†</sup>
		GS [3]	HIO [4]	$\xi$ -Encoded <sup>†</sup>		$(y \rightarrow \alpha)$ <sup>†</sup>	$(y \rightarrow \phi)$ <sup>†</sup>	
Circle	Noiseless	0.996 ± 0.011	0.996 ± 0.014	0.993 ± 0.033	0.906 ± 0.096	0.913 ± 0.095	0.907 ± 0.110	0.928 ± 0.087
	Noisy	<u>0.919 ± 0.033</u>	0.901 ± 0.055	0.986 ± 0.015	0.876 ± 0.122	0.887 ± 0.114	0.899 ± 0.109	0.869 ± 0.132
Triangle	Noiseless	0.992 ± 0.017	1.000 ± 0.000	0.989 ± 0.031	0.979 ± 0.036	0.987 ± 0.030	0.989 ± 0.028	0.996 ± 0.004
	Noisy	0.900 ± 0.037	0.881 ± 0.062	0.981 ± 0.22	0.972 ± 0.027	0.971 ± 0.034	<u>0.973 ± 0.028</u>	0.965 ± 0.040
Pentagon	Noiseless	0.991 ± 0.012	1.000 ± 0.005	0.993 ± 0.017	0.979 ± 0.034	0.996 ± 0.009	0.996 ± 0.010	0.997 ± 0.003
	Noisy	0.912 ± 0.033	0.893 ± 0.057	0.983 ± 0.015	0.940 ± 0.081	0.941 ± 0.079	<u>0.944 ± 0.077</u>	0.936 ± 0.079
Task: Wavefront estimation (trivial ambiguities do matter). Metric: Strehl ratio.								
Circle	Noiseless	0.582 ± 0.379	0.605 ± 0.384	0.563 ± 0.372	0.533 ± 0.261	0.536 ± 0.270	0.529 ± 0.278	0.630 ± 0.274
	Noisy	0.141 ± 0.070	<u>0.148 ± 0.076</u>	0.489 ± 0.285	0.543 ± 0.225	<u>0.549 ± 0.234</u>	0.551 ± 0.241	0.545 ± 0.205
Triangle	Noiseless	0.847 ± 0.294	1.000 ± 0.000	0.847 ± 0.028	0.913 ± 0.074	0.954 ± 0.063	0.958 ± 0.060	0.976 ± 0.019
	Noisy	0.155 ± 0.067	0.157 ± 0.069	0.664 ± 0.233	0.837 ± 0.086	<u>0.828 ± 0.091</u>	0.827 ± 0.091	0.801 ± 0.103
Pentagon	Noiseless	0.633 ± 0.379	0.998 ± 0.036	0.645 ± 0.370	0.928 ± 0.080	0.983 ± 0.026	0.983 ± 0.028	0.985 ± 0.019
	Noisy	0.136 ± 0.067	0.145 ± 0.073	0.508 ± 0.285	0.779 ± 0.179	0.767 ± 0.196	<u>0.770 ± 0.190</u>	0.736 ± 0.190
Task: Computation speed on 128 × 128 PSF. Metric: 1 / Time to recover the phase (Hz.)								
Speed (Hz.)		3.33	2.38	0.31	5200	<u>3700</u>	3300	440

## V. EXPERIMENTS

To help further distinguish between the problem of phase retrieval and wavefront estimation, we will compare the performance of various algorithms on each problem. As we will see, high performance in phase retrieval does not always transfer to wavefront estimation. We additionally built a prototype triangle pupil system and discuss some results.

### A. Simulation setting

Our simulated experiments consist of drawing i.i.d. uniform random variables for Zernike coefficients in  $\alpha$ ,  $\alpha_i \sim U(-2, 2)$ , with  $\phi$  formed by a weighted sum of the Zernike polynomials and windowed by the corresponding  $\mathbf{p}$ . The PSF  $\mathbf{y}$  is then generated and noise is optionally added and clipped as  $\max(\mathbf{y} + \mathbf{n}, 0)$  where  $\mathbf{n} \sim \mathcal{N}(0, \sigma^2 \mathbf{I})$ . We choose  $\mathbf{p}$  for all shapes to (approximately) have the same amount of support pixels to keep resolution consistent.

Regarding noise level, a PSF is highly concentrated in the center of the grid, making a typical signal-to-noise ratio (SNR) calculation potentially misleading. The noisy case reported in Table I has an SNR of  $-1$  dB when computed over the center  $60 \times 60$  crop and  $-7.5$  dB over the entire  $128 \times 128$  grid. The S2P and related methods can operate directly on this center crop, allowing them some flexibility to ignore noise beyond the typical support of a PSF. For fairness, we remove the noise beyond the  $60 \times 60$  crop when using the GS/HIO algorithms.

### B. Discussion of simulated results

In Table I we compare performance across algorithms on phase retrieval and wavefront estimation. Following [7], we use the metric of normalized correlation  $\mathbf{y}^T \hat{\mathbf{y}} / \|\mathbf{y}\| \|\hat{\mathbf{y}}\|$  for phase retrieval and the Strehl ratio (12) for wavefront

estimation. Hence, both metrics vary in the range of  $[0, 1]$ , with 1 meaning perfect recovery for the relevant task. We report mean and standard deviation on a testing dataset of 1000 PSFs.

We summarize Table I as follows:

- 1) **Iterative methods.** Iterative methods perform well on the noiseless phase retrieval task, even when the underlying phase has ambiguity (see circle performance). The  $\xi$ -encoded method is best in the presence of noise. Performance on wavefront estimation is mixed; if the objective landscape is highly non-convex than the recovery is suboptimal. The HIO algorithm performs well in the noiseless case for both problems with the exception of circular support (due to ambiguity).
- 2) **Direct methods.** Direct PSF inversion performs well on phase retrieval when the underlying problem is unambiguous; ambiguity appears to slightly impact performance on the phase retrieval problem. Direct methods perform better on wavefront estimation methods compared to their iterative counterparts, especially in the noisy case. The S2P is more robust in noise while the direct PSF alternatives perform better in the noiseless case (likely due to the use of basis representation).
- 3) **Unrolled S2P.** The unrolled S2P tends to perform the best of the supervised methods on the phase retrieval and wavefront estimation tasks in the noiseless case. It is interesting to note that the performance is slightly worse on noisy wavefront estimation against direct PSF inversion, which we hypothesize is due to overparameterization or the iterative mechanism allowing it to (erroneously) fit the noise.

We also report speeds of the various algorithms in Table I, where for iterative methods we have used 500 iterations for

TABLE II  
COMPARISON OF ( $\mathbf{y} \rightarrow \phi$ ) PERFORMANCE BETWEEN TABLE I AND SELF-SUPERVISED APPROACHES (NOISELESS CONDITIONS)

Task: Phase retrieval. Metric: Normalized correlation.		
Support	Supervised (Table I)	Semi-Supervised
Circle	$0.907 \pm 0.110$	$0.991 \pm 0.011$
Triangle	$0.989 \pm 0.028$	$0.988 \pm 0.020$
Pentagon	$0.996 \pm 0.010$	$0.982 \pm 0.031$
Task: Wavefront estimation. Metric: Strehl ratio.		
Support	Supervised (Table I)	Semi-Supervised
Circle	$0.529 \pm 0.278$	$0.563 \pm 0.333$
Triangle	$0.958 \pm 0.060$	$0.822 \pm 0.073$
Pentagon	$0.983 \pm 0.028$	$0.587 \pm 0.287$

the HIO/GS algorithm and 300 iterations for the  $\xi$ -encoded INR. The S2P performs approximately  $2000\times$  faster than the GS/HIO algorithms and nearly  $5\times$  the speed of the high-speed Shack-Hartmann wavefront sensor from Thor labs. In turbulence correction, the speed for optical correction can be on the scale of tens to hundreds of Hertz [1], only the Shack-Hartmann sensor and our methods meet this requirement.

We offer a comparison between supervised and self-supervised training, that is

$$\operatorname{argmin}_{\theta} \left\| \mathbf{y} - \left| \mathbf{F} \left( \mathbf{p} \odot e^{jg_{\theta}(\mathbf{y})} \right) \right|^2 \right\|^2, \quad (19)$$

for the direct mapping ( $\mathbf{y} \rightarrow \phi$ ) in Table II. The triangle pupil performs best for wavefront estimation, highlighting the concept of *identifiability* in the wavefront estimation problem; we empirically observe this to be related to the degree of pupil asymmetry (similar to iterative algorithms). The improvement for phase retrieval using a circular pupil is likely due to its ability to ignore ambiguity when trained in a self-supervised manner.

### C. Real experiments

A prototype triangular pupil imaging system with a spatial light modulator (SLM) was built as shown in Figure 9. We use a Holoeye LC 2012 SLM with a 520 nm. laser and record PSFs with a Teledyne Imaging FLIR Grasshopper 3.

Due to limitations in the system/optics we are able to utilize only  $22 \times 22$  pixels for the SLM pattern (see Figure 9 for a visualization of the pupil size) hence our patterns contain only the first 10 Zernike polynomials to avoid aliasing. Due to a slight mismatch between simulated and real data, we train a network on real data only, leaving some for validation. We train a network  $g_{\theta}(\mathbf{y}) \approx \alpha$  on 135 PSF and phase pairs, and perform validation on the remaining 15. A few examples of real measurements, the phase aberration, and recovery, along with Zernike coefficients are shown in Figure 10.

## VI. CONCLUSION

In this work we studied the problem of wavefront estimation. We showed that trivial ambiguities play an important role in determining the uniqueness of the solution. We identified a set of conditions under which we can guarantee a unique

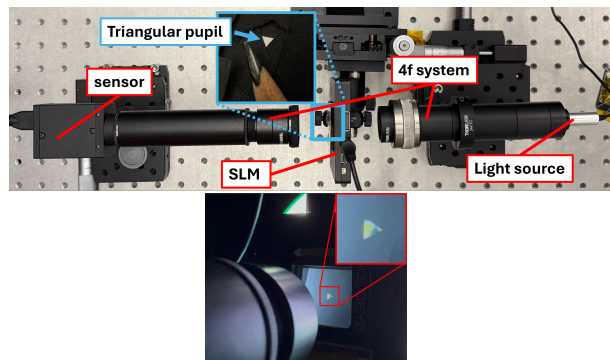


Fig. 9. Real experiment setup. [Top] The 4f-system, SLM, and triangular pupil setup. [Bottom] Visualization of triangular pattern on SLM.

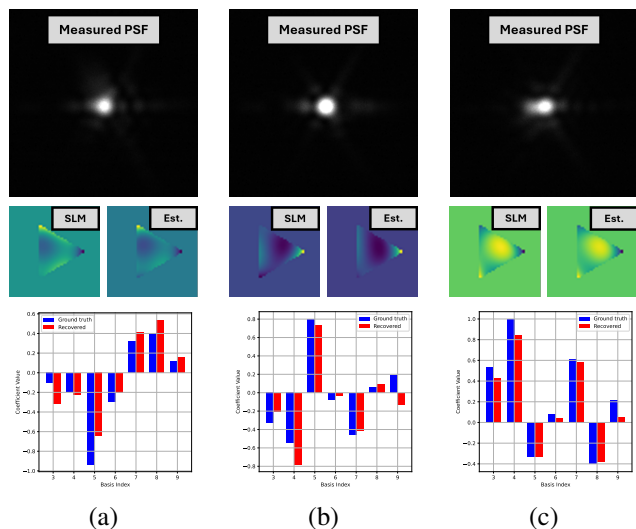


Fig. 10. Evaluation on *real* validation data. [Top] Measured PSFs. [Middle] SLM phase pattern (left) and estimated phase (right) for each case. [Bottom] Basis coefficient comparison (blue as ground truth, red as recovered). All cases shown (a-c) are validation data. Here we use the MLP-1 method, hence runtime is  $\sim 3700$  Hz.

recovery of the phase. We proposed several algorithms inspired by previous approaches to recover phases from their PSFs in real time and demonstrated our methodology in a real system using an SLM.

With this new approach, we envision that it shall play a role in achieving fast and accurate wavefront estimation in a passive setting, opening the door to a new generation of medical and defense applications. In future works, we look towards answering questions related to robustness and performance bounds as well as optimal pupil geometry and algorithm co-design.

### ACKNOWLEDGMENTS

The authors thank Harshana Weligampola for the helpful discussions and assistance in the optical bench setup.

### PROOF OF THEOREM 2

*Proof.* Using the Cauchy-Schwarz inequality we may write

$$|\mathbf{x}^H \hat{\mathbf{x}}|^2 \leq (\mathbf{x}^H \mathbf{x})(\hat{\mathbf{x}}^H \hat{\mathbf{x}}).$$

With the Cauchy-Schwarz inequality, equality is achieved if and only if  $\hat{\mathbf{x}}$  is a complex, scalar multiple of  $\mathbf{x}$ . This implies

$$\hat{\mathbf{x}} = \nu \mathbf{x},$$

where  $\nu \in \mathbb{C}$ . Furthermore, since  $\hat{\mathbf{x}} \in \Omega(\mathbf{x})$ ,  $\nu = e^{jc}$ , where  $c \in [0, 2\pi)$  can be shown from noting the periodicity of the complex exponential. Hence the Theorem follows.  $\square$

### PROOF OF THEOREM 3

#### Proofs of Lemmas

We now present three Lemmas that help to remove certain sets of trivial ambiguities. Recall that we have assumed that  $\mathbf{p}$  is known exactly, hence we shall heavily rely upon the knowledge of  $\mathbf{p}$ . Specifically, by definition of the support and since it is known *a priori*, we can require that

$$\mathbf{p} \odot \hat{\mathbf{x}} = \hat{\mathbf{x}} \quad (20)$$

for any candidate  $\hat{\mathbf{x}} \in \Omega(\mathbf{x})$ . This will help to eliminate most of the ambiguities.

Lemma 1 is aimed at removing  $\mathcal{T}_{\text{shift}}$  for  $\ell \neq \mathbf{0}$ .

**Lemma 1** (Aperiodic support). *Let  $\mathbf{p}$  is known and  $|x[\mathbf{n}]| > 0 \forall \mathbf{n} \in \mathbb{Z}_N$ . If  $\nexists \ell \in \mathbb{Z}_N$  with  $\ell \neq \mathbf{0}$  such that  $p[\mathbf{n} - \ell] = p[\mathbf{n}] \forall \mathbf{n} \in \mathbb{Z}_N$ , then  $\mathbf{p} \odot \mathcal{T}_{\text{shift}}(\mathbf{x}) \notin \Omega(\mathbf{x}) \forall \ell \neq \mathbf{0} \in \mathbb{Z}_N$ .*

*Proof.* Suppose  $\mathbf{p}$  is known and  $\nexists \ell \in \mathbb{Z}_N$  for  $\ell \neq \mathbf{0}$  such that  $p[\mathbf{n} - \ell] = p[\mathbf{n}]$  and  $\mathcal{T}_{\text{shift}}(\mathbf{x}) \in \Omega(\mathbf{x})$ . Since  $x[\mathbf{n} - \ell]$  is an ambiguity by translation, its support too must be a translation. Hence, by definition of  $\mathbf{p}$ ,

$$p[\mathbf{n} - \ell]x[\mathbf{n} - \ell] = x[\mathbf{n} - \ell], \quad \forall \mathbf{n} \in \mathbb{Z}_N.$$

Since we know  $\mathbf{p}$ , the solution must also satisfy

$$p[\mathbf{n}]p[\mathbf{n} - \ell]x[\mathbf{n} - \ell] = x[\mathbf{n} - \ell], \quad \forall \mathbf{n} \in \mathbb{Z}_N.$$

However, this would imply  $p[\mathbf{n}]p[\mathbf{n} - \ell] = 1 \forall \mathbf{n} \in \mathbb{Z}_N$  for some  $\ell \neq \mathbf{0}$  since  $|x[\mathbf{n}]| > 0 \forall \mathbf{n} \in \mathbb{Z}_N$  which contradicts our assumption. By contradiction, the Lemma follows.  $\square$

Lemma 2 is aimed at eliminating  $\mathcal{T}_{\text{shift}} \circ \mathcal{T}_{\text{flip}}$ . Note that this also eliminates  $\mathcal{T}_{\text{flip}}$  if we consider a shift of  $\ell = \mathbf{0}$ .

**Lemma 2** (Asymmetric and aperiodic support). *Let  $\mathbf{p}$  be known and  $|x[\mathbf{n}]| > 0 \forall \mathbf{n} \in \mathbb{Z}_N$ . Then  $\exists \ell \in \mathbb{Z}_N$  such that  $\mathbf{p} \odot (\mathcal{T}_{\text{shift}} \circ \mathcal{T}_{\text{flip}})(\mathbf{x}) \in \Omega(\mathbf{x})$  if and only if  $(\mathcal{T}_{\text{shift}} \circ \mathcal{T}_{\text{flip}})(\mathbf{p}) = \mathbf{p}$  for the same  $\ell$ .*

*Proof.* ( $\implies$ ). Suppose  $\exists \ell \in \mathbb{Z}_N$  such that  $(\mathcal{T}_{\text{shift}} \circ \mathcal{T}_{\text{flip}})(\mathbf{x}) \in \Omega(\mathbf{x})$ . Then

$$p[-\mathbf{n} - \ell]x^*[-\mathbf{n} - \ell] = x^*[-\mathbf{n} - \ell].$$

Since  $\mathbf{p}$  is known, this also implies

$$p[\mathbf{n}]p[-\mathbf{n} - \ell]x^*[-\mathbf{n} - \ell] = x^*[-\mathbf{n} - \ell]$$

which further implies  $p[\mathbf{n}]p[-\mathbf{n} - \ell] = 1 \forall \mathbf{n} \in \mathbb{Z}_N$  since  $|x[\mathbf{n}]| > 0 \forall \mathbf{n} \in \mathbb{Z}_N$ . By definition of  $\mathbf{p}$ , this implies  $p[\mathbf{n}] = p[-\mathbf{n} - \ell]$  for all  $\mathbf{n} \in \mathbb{Z}_N$ .

( $\impliedby$ ). Suppose  $\exists \ell \in \mathbb{Z}_N$  such that  $(\mathcal{T}_{\text{shift}} \circ \mathcal{T}_{\text{flip}})(\mathbf{p}) = \mathbf{p}$ . Consider a transformation of the true solution  $\mathbf{x}$ :  $(\mathcal{T}_{\text{shift}} \circ \mathcal{T}_{\text{flip}})(\mathbf{x})$ . Then the following holds  $\forall \mathbf{n} \in \mathbb{Z}_N$ :

$$\begin{aligned} p[-\mathbf{n} - \ell]x^*[-\mathbf{n} - \ell] &= x^*[-\mathbf{n} - \ell] \\ \implies p[\mathbf{n}]x^*[-\mathbf{n} - \ell] &= x^*[-\mathbf{n} - \ell]. \end{aligned}$$

Hence,  $\mathbf{p} \odot (\mathcal{T}_{\text{shift}} \circ \mathcal{T}_{\text{flip}})(\mathbf{x}) \in \Omega(\mathbf{x})$ .

( $\iff$ ). Follows from both directions.  $\square$

The final Lemma is aimed at eliminating  $\mathcal{T}_{\text{dc}}$ .

**Lemma 3** (Known complex DC shift). *Let  $|x[\mathbf{n}]| > 0 \forall \mathbf{n} \in \mathbb{Z}_N$ . If  $\phi^T \mathbf{p} / \|\mathbf{p}\| = c_0$  with  $c_0 \in [0, 2\pi) \implies \nexists c' \in (0, 2\pi)$  such that  $\mathbf{x} = e^{jc'} \mathbf{x}$ .*

*Proof.* We first expand

$$\phi[\mathbf{n}] = c_0 + \tilde{\phi}[\mathbf{n}], \quad \forall \mathbf{n} \in \mathbb{Z}_N$$

and let  $\mathbf{p}^T \phi / \|\mathbf{p}\| = c_0$  and  $\mathbf{p}^T \tilde{\phi} / \|\mathbf{p}\| = 0$ . Then  $\forall \mathbf{n} \in \mathbb{Z}_N$ ,

$$x[\mathbf{n}] = e^{jc_0} |x[\mathbf{n}]| e^{j\tilde{\phi}[\mathbf{n}]}$$

Now suppose  $\exists c' \in (0, 2\pi)$  such that  $\mathbf{x} = e^{jc'} \mathbf{x}$ . Since  $|\mathbf{x}| > \mathbf{0}$ , this implies  $e^{j(c_0+c')} = e^{jc_0}$  which further implies

$$e^{jc'} = 1, \quad c' \in (0, 2\pi).$$

This can not be true, hence the Lemma is shown.  $\square$

#### Proof of Theorem 3

*Proof.* Define  $\mathbf{y} \in \mathbb{R}^K$  as vector according to measurement model (3) and further suppose that there exists no non-trivial ambiguity, i.e.,  $\nexists \hat{\mathbf{x}} \notin \Omega(\mathbf{x})$  such that  $\mathbf{y} = |\mathbf{F}\hat{\mathbf{x}}|^2$ . Further suppose we meet the conditions specified of Theorem 3. Note that we have not yet asserted Hayes' Theorem.

Recall that the set of trivial ambiguities relative to true solution  $\mathbf{x}$  is as follows:

$$\Omega(\mathbf{x}) = \langle \{\mathcal{T}_{\text{dc}}(\mathbf{x}), \mathcal{T}_{\text{shift}}(\mathbf{x}), \mathcal{T}_{\text{flip}}(\mathbf{x})\} \rangle.$$

By applying Lemma 3, which provides uniqueness relative to  $\mathcal{T}_{\text{dc}}$  applied through condition (iii),  $\Omega(\mathbf{x})$  can be shown to reduce to

$$\begin{aligned} \Omega(\mathbf{x}) &= \langle \{\mathcal{T}_{\text{shift}}(\mathbf{x}), \mathcal{T}_{\text{flip}}(\mathbf{x})\} \rangle \\ &= \langle \{\mathcal{T}_{\text{shift}}(\mathbf{x}), \mathcal{T}_{\text{flip}}(\mathbf{x}), (\mathcal{T}_{\text{shift}} \circ \mathcal{T}_{\text{flip}})(\mathbf{x})\} \rangle. \end{aligned}$$

By Lemma 2, which eliminates ambiguities related to the flipped solution facilitated by conditions (i) and (ii), this further can be shown to reduce to

$$\Omega(\mathbf{x}) = \langle \mathcal{T}_{\text{shift}}(\mathbf{x}) \rangle.$$

By Lemma 1, related to the shift ambiguity and applied via condition (i) and (ii),  $\mathcal{T}_{\text{shift}}$  is eliminated for all  $\ell \in \mathbb{Z}_N$  such that  $\ell \neq \mathbf{0}$ . Therefore, the application of Lemma 1 leads to

$$\Omega(\mathbf{x}) = \langle \mathbf{x} \rangle,$$

i.e., the only remaining solution is indeed  $\mathbf{x}$ .

Hence, if no non-trivial ambiguities exist, under conditions stated in Theorem 3 the solution is unique. To arrive at Theorem 3, one need only require  $\mathbf{y}$  to satisfy Hayes' Theorem (and accordingly a non-trivial ambiguity occurs with probability 0), and the Theorem follows.  $\square$

## PROOF OF THEOREM 4

*Proof.* Let  $\psi[\mathbf{n}]$  be known over  $c[\mathbf{n}]$  and  $y[\mathbf{n}]$  satisfy Hayes' Theorem, hence, all ambiguous solutions (with probability 1) belong to the set of trivial ambiguities  $\Omega(\mathbf{x})$  where  $x[\mathbf{n}] = p[\mathbf{n}]e^{j\psi[\mathbf{n}]}$  is the true solution.

Suppose there exists another support  $\hat{\mathbf{p}} \neq \mathbf{p}$  such that  $\hat{p}[\mathbf{n}]e^{j\psi[\mathbf{n}]} \in \Omega(\mathbf{x})$ . It can be observed by the definition of  $\Omega(\mathbf{x})$  that the magnitudes of all solutions that belong to  $\Omega(\mathbf{x})$  are of the form of translations and flips of  $\mathbf{p}$ . Therefore,  $\hat{p}[\mathbf{n}] = p[\pm\mathbf{n} + \ell]$  for some  $\ell \in \mathbb{Z}_N$ . Since  $\psi$  is also known, this implies  $p[\pm\mathbf{n} + \ell]e^{j\psi[\mathbf{n}]} \in \Omega(\mathbf{x})$ .

One can then observe that there does exist  $\ell \in \mathbb{Z}_N$  such that  $\hat{\mathbf{p}} \neq \mathbf{p}$  and  $p[\pm\mathbf{n} + \ell]e^{j\psi[\mathbf{n}]} \in \Omega(\mathbf{x})$ . This represents the contrapositive case, thus the Theorem follows.  $\square$

## REFERENCES

- [1] R. K. Tyson and B. W. Frazier, *Principles of Adaptive Optics*, CRC Press, 2022, [Taylor-Francis URL](#).
- [2] D. Sayre, "Some implications of a theorem due to Shannon," *Acta Crystallographica*, vol. 5, no. 6, pp. 843, Nov 1952, [IUCr URL](#).
- [3] R. W. Gerchberg and W. O. Saxton, "A practical algorithm for the determination of phase from image and diffraction plane pictures," *Optik*, vol. 35, pp. 237–246, 1972.
- [4] J. R. Fienup, "Phase retrieval algorithms: a comparison," *Applied Optics*, vol. 21, no. 15, pp. 2758–2769, 1982, [Optica URL](#).
- [5] K. Jaganathan, Y. C. Eldar, and B. Hassibi, "Phase retrieval: An overview of recent developments," *Optical Compressive Imaging*, pp. 279–312, 2016, [Taylor-Francis URL](#).
- [6] T. Bendory, R. Beinert, and Y. C. Eldar, "Fourier phase retrieval: Uniqueness and algorithms," in *Compressed Sensing and its Applications: Second International MATHEON Conference 2015*. Springer, 2017, pp. 55–91, [Springer URL](#).
- [7] J. Dong, L. Valzania, A. Maillard, T.-a. Pham, S. Gigan, and M. Unser, "Phase retrieval: From computational imaging to machine learning: A tutorial," *IEEE Signal Processing Magazine*, vol. 40, no. 1, pp. 45–57, 2023, [IEEE Xplore](#).
- [8] J. Ranieri, A. Chebira, Y. M. Lu, and M. Vetterli, "Phase retrieval for sparse signals: Uniqueness conditions," 2013, [arXiv:1308.3058](#).
- [9] Y. C. Eldar, P. Sidorenko, D. G. Mixon, S. Barel, and O. Cohen, "Sparse phase retrieval from short-time Fourier measurements," *IEEE Signal Processing Letters*, vol. 22, no. 5, pp. 638–642, 2014, [IEEE Xplore](#).
- [10] R. A. Gonsalves, "Phase retrieval and diversity in adaptive optics," *Optical Engineering*, vol. 21, no. 5, pp. 829–832, 1982, [SPIE URL](#).
- [11] E. J. Candès, X. Li, and M. Soltanolkotabi, "Phase retrieval from coded diffraction patterns," *Applied and Computational Harmonic Analysis*, vol. 39, no. 2, pp. 277–299, 2015, [ScienceDirect URL](#).
- [12] R. Ragazzoni, "Pupil plane wavefront sensing with an oscillating prism," *Journal of Modern Optics*, vol. 43, no. 2, pp. 289–293, 1996, [Taylor-Francis URL](#).
- [13] P. Hariharan, B. F. Oreb, and T. Eiju, "Digital phase-shifting interferometry: a simple error-compensating phase calculation algorithm," *Applied Optics*, vol. 26, no. 13, pp. 2504–2506, Jul 1987, [Optica URL](#).
- [14] M. M. Colavita, "Limitations to optical/IR interferometry from the ground and space," in *Very High Angular Resolution Imaging*. 1994, pp. 469–476, Springer Netherlands, [Springer URL](#).
- [15] J. C. Wyant, "Dynamic interferometry," *Optics & Photonics News*, vol. 14, no. 4, pp. 36–41, Apr 2003, [Optica URL](#).
- [16] B. Y. Feng, H. Guo, M. Xie, V. Boominathan, M. K. Sharma, A. Veeraraghavan, and C. A. Metzler, "NeuWS: Neural wavefront shaping for guide-star-free imaging through static and dynamic scattering media," *Science Advances*, vol. 9, no. 26, pp. eadg4671, 2023, [Science URL](#).
- [17] M. H. Hayes, "The reconstruction of a multidimensional sequence from the phase or magnitude of its Fourier transform," *IEEE Transactions on Acoustics, Speech, and Signal Processing*, vol. 30, no. 2, pp. 140–154, 1982, [IEEE Xplore](#).
- [18] J. R. Fienup, "Reconstruction of objects having latent reference points," *Journal of the Optical Society of America*, vol. 73, no. 11, pp. 1421–1426, Nov 1983, [Optica URL](#).
- [19] T. R. Crimmins and J. R. Fienup, "Uniqueness of phase retrieval for functions with sufficiently disconnected support," *Journal of the Optical Society of America*, vol. 73, no. 2, Feb 1983, [Optica URL](#).
- [20] A. S. Bandeira, J. Cahill, D. G. Mixon, and A. A. Nelson, "Saving phase: Injectivity and stability for phase retrieval," *Applied and Computational Harmonic Analysis*, vol. 37, no. 1, pp. 106–125, 2014, [ScienceDirect URL](#).
- [21] A. Conca, D. Edidin, M. Hering, and C. Vinzant, "An algebraic characterization of injectivity in phase retrieval," *Applied and Computational Harmonic Analysis*, vol. 38, no. 2, pp. 346–356, 2015, [ScienceDirect URL](#).
- [22] C. Vinzant, "A small frame and a certificate of its injectivity," in *2015 International Conference on Sampling Theory and Applications (SampTA)*, 2015, pp. 197–200, [IEEE Xplore](#).
- [23] M. H. Hayes and J. H. McClellan, "Reducible polynomials in more than one variable," *Proceedings of the IEEE*, vol. 70, no. 2, pp. 197–198, 1982, [IEEE Xplore](#).
- [24] J. R. Fienup and C. C. Wackerman, "Phase-retrieval stagnation problems and solutions," *Journal of the Optical Society of America A*, vol. 3, no. 11, pp. 1897–1907, 1986, [Optica URL](#).
- [25] J. R. Fienup and C. Dainty, "Phase retrieval and image reconstruction for astronomy," *Image Recovery: Theory and Application*, vol. 231, pp. 275, 1987, [URL](#).
- [26] J. H. Seldin and J. R. Fienup, "Numerical investigation of the uniqueness of phase retrieval," *Journal of the Optical Society of America A*, vol. 7, no. 3, pp. 412–427, 1990, [Optica URL](#).
- [27] R. G. Paxman, T. J. Schulz, and J. R. Fienup, "Joint estimation of object and aberrations by using phase diversity," *Journal of the Optical Society of America A*, vol. 9, no. 7, pp. 1072–1085, 1992, [Optica URL](#).
- [28] D. Sayre, "X-ray crystallography: the past and present of the phase problem," *Journal of Structural Chemistry*, vol. 13, pp. 81–96, 2002, [Springer URL](#).
- [29] G. Oszlányi and A. Sütö, "Ab initio structure solution by charge flipping," *Acta Crystallographica Section A*, vol. 60, no. 2, pp. 134–141, Mar 2004, [IUCr URL](#).
- [30] L. Palatinus, "The charge-flipping algorithm in crystallography," *Acta Crystallographica Section B*, vol. 69, no. 1, pp. 1–16, Feb 2013, [IUCr URL](#).
- [31] L.-H. Yeh, L. Tian, Z. Liu, M. Chen, J. Zhong, and L. Waller, "Experimental robustness of Fourier ptychographic phase retrieval algorithms," in *Imaging and Applied Optics 2015*. 2015, p. CW4E.2, Optica Publishing Group, [Optica URL](#).
- [32] E. J. Candès, X. Li, and M. Soltanolkotabi, "Phase retrieval via wirtinger flow: Theory and algorithms," *IEEE Transactions on Information Theory*, vol. 61, no. 4, pp. 1985–2007, 2015, [IEEE Xplore](#).
- [33] M. Guizar-Sicairos and J. R. Fienup, "Phase retrieval with transverse translation diversity: a nonlinear optimization approach," *Optics Express*, vol. 16, no. 10, pp. 7264–7278, May 2008, [Optica URL](#).
- [34] E. J. Candès, T. Strohmer, and V. Voroninski, "PhaseLift: Exact and stable signal recovery from magnitude measurements via convex programming," *Communications on Pure and Applied Mathematics*, vol. 66, no. 8, pp. 1241–1274, 2013, [Wiley URL](#).
- [35] E. J. Candès, Y. C. Eldar, T. Strohmer, and V. Voroninski, "Phase retrieval via matrix completion," *SIAM Journal on Imaging Sciences*, vol. 6, no. 1, pp. 199–225, 2013, [SIAM URL](#).
- [36] K. Jaganathan, S. Oymak, and B. Hassibi, "Recovery of sparse 1-D signals from the magnitudes of their Fourier transform," in *2012 IEEE International Symposium on Information Theory Proceedings*, 2012, pp. 1473–1477, [IEEE Xplore](#).
- [37] T. Goldstein and C. Studer, "PhaseMax: Convex phase retrieval via basis pursuit," *IEEE Transactions on Information Theory*, vol. 64, no. 4, pp. 2675–2689, 2018, [IEEE Xplore](#).
- [38] I. Waldspurger, A. d'Aspremont, and S. Mallat, "Phase recovery, MaxCut and complex semidefinite programming," *Mathematical Programming*, vol. 149, pp. 47–81, 2015, [Springer URL](#).
- [39] W. Luo, W. Alghamdi, and Y. M. Lu, "Optimal spectral initialization for signal recovery with applications to phase retrieval," *IEEE Transactions on Signal Processing*, vol. 67, no. 9, pp. 2347–2356, 2019, [IEEE Xplore](#).
- [40] A. Maillard, F. Krzakala, Y. M. Lu, and L. Zdeborova, "Construction of optimal spectral methods in phase retrieval," in *Proceedings of the 2nd Mathematical and Scientific Machine Learning Conference*. 16–19 Aug 2022, vol. 145 of *Proceedings of Machine Learning Research*, pp. 693–720, PMLR, [PMLR URL](#).
- [41] L. Valzania, J. Dong, and S. Gigan, "Accelerating ptychographic reconstructions using spectral initializations," *Optics Letters*, vol. 46, no. 6, pp. 1357–1360, Mar 2021, [Optica URL](#).
- [42] P. Schniter, S. Rangan, and A. K. Fletcher, "Vector approximate message passing for the generalized linear model," in *2016 50th Asilomar Conference on Signals, Systems and Computers*, 2016, pp. 1525–1529, [IEEE Xplore](#).

- [43] M. Mezard and A. Montanari, *Information, Physics, and Computation*, Oxford University Press, 2009, [Oxford Academic URL](#).
- [44] I. Johnson, K. Jefimovs, O. Bunk, C. David, M. Dierolf, J. Gray, D. Renker, and F. Pfeiffer, “Coherent diffractive imaging using phase front modifications,” *Physical Review Letters*, vol. 100, pp. 155503, Apr 2008, [APS URL](#).
- [45] A. Levin, R. Fergus, F. Durand, and W. T. Freeman, “Image and depth from a conventional camera with a coded aperture,” *ACM transactions on graphics (TOG)*, vol. 26, no. 3, pp. 70, 2007, [ACM URL](#).
- [46] E. G. Loewen and E. Popov, *Diffraction Gratings and Applications*, CRC Press, 1st edition, 1997, [Taylor-Francis URL](#).
- [47] M. S. Asif, A. Ayremlou, A. Sankaranarayanan, A. Veeraraghavan, and R. G. Baraniuk, “FlatCam: Thin, lensless cameras using coded aperture and computation,” *IEEE Transactions on Computational Imaging*, vol. 3, no. 3, pp. 384–397, 2016, [IEEE Xplore](#).
- [48] A. Faridian, D. Hopp, G. Pedrini, U. Eigenhaller, M. Hirscher, and W. Osten, “Nanoscale imaging using deep ultraviolet digital holographic microscopy,” *Optics Express*, vol. 18, no. 13, pp. 14159–14164, Jun 2010, [Optica URL](#).
- [49] M. Xie, H. Guo, B. Y. Feng, L. Jin, A. Veeraraghavan, and C. A. Metzler, “WaveMo: Learning wavefront modulations to see through scattering,” in *Proceedings of the IEEE/CVF Conference on Computer Vision and Pattern Recognition*, 2024, pp. 25276–25285, [IEEE Xplore](#).
- [50] U. S. Kamilov, C. A. Bouman, G. T. Buzzard, and B. Wohlberg, “Plug-and-play methods for integrating physical and learned models in computational imaging: Theory, algorithms, and applications,” *IEEE Signal Processing Magazine*, vol. 40, no. 1, pp. 85–97, 2023, [IEEE Xplore](#).
- [51] P. Hand, O. Leong, and V. Voroninski, “Phase retrieval under a generative prior,” in *Advances in Neural Information Processing Systems*, 2018, pp. 9154–9164, [ACM URL](#).
- [52] P. Bohra, T.-a. Pham, J. Dong, and M. Unser, “Bayesian inversion for nonlinear imaging models using deep generative priors,” *IEEE Transactions on Computational Imaging*, vol. 8, pp. 1237–1249, 2022, [IEEE Xplore](#).
- [53] C. A. Metzler, P. Schniter, and A. Veeraraghavan, “prDeep: Robust phase retrieval with a flexible deep network,” in *International Conference on Machine Learning*, 2018, pp. 3501–3510, [PMLR URL](#).
- [54] A. Kappeler, S. Ghosh, J. Holloway, O. Cossairt, and A. Katsaggelos, “Ptychnet: CNN based Fourier ptychography,” in *IEEE International Conference on Image Processing (ICIP)*, 2017, p. 1712–1716, [IEEE Xplore](#).
- [55] K. Wang, L. Song, C. Wang, Z. Ren, G. Zhao, J. Dou, J. Di, G. Barbastathis, R. Zhou, J. Zhao, and E. Y. Lam, “On the use of deep learning for phase recovery,” *Light: Science and Applications*, vol. 13, no. 4, pp. 1–46, 2024, [Nature URL](#).
- [56] R. J. Noll, “Zernike polynomials and atmospheric turbulence,” *Journal of the Optical Society of America*, vol. 66, no. 3, pp. 207–211, 1976, [Optica URL](#).
- [57] S. H. Chan and N. Chimitt, “Computational imaging through atmospheric turbulence,” *Foundations and Trends® in Computer Graphics and Vision*, vol. 15, no. 4, pp. 253–508, 2023, [NOW Publishers URL](#).
- [58] J. R. Fienup, T. R. Crimmins, and W. Holsztynski, “Reconstruction of the support of an object from the support of its autocorrelation,” *Journal of the Optical Society of America*, vol. 72, no. 5, pp. 610–624, May 1982, [Optica URL](#).
- [59] J. N. Cederquist, J. R. Fienup, C. C. Wackerman, S. R. Robinson, and D. Kryskowski, “Wave-front phase estimation from Fourier intensity measurements,” *Journal of the Optical Society of America A*, vol. 6, no. 7, pp. 1020–1026, 1989, [Optica URL](#).
- [60] J. R. Fienup, “Phase retrieval using boundary conditions,” *Journal of the Optical Society of America A*, vol. 3, no. 2, pp. 284–288, Feb 1986, [Optica URL](#).
- [61] F. Martinache, “The asymmetric pupil Fourier wavefront sensor,” *Publications of the Astronomical Society of the Pacific*, vol. 125, no. 926, pp. 422, 2013, [IOPScience URL](#).
- [62] R. G. Paxman, D. A. Carrara, J. J. Miller, K. W. Gleichman, M. A. Rucci, and B. K. Karch, “Estimation ambiguities encountered when imaging through turbulence,” in *Unconventional and Indirect Imaging, Image Reconstruction, and Wavefront Sensing 2019*. 2019, vol. 11135, p. 111350G, SPIE, [SPIE URL](#).
- [63] K. Tayal, C.-H. Lai, R. Manekar, Z. Zhuang, V. Kumar, and J. Sun, “Unlocking inverse problems using deep learning: Breaking symmetries in phase retrieval,” in *NeurIPS 2020 Workshop on Deep Learning and Inverse Problems*, 2020, [OpenReview URL](#).
- [64] R. Manekar, K. Tayal, Z. Zhuang, C.-H. Lai, V. Kumar, and J. Sun, “Breaking symmetries in data-driven phase retrieval,” in *OSA Imaging and Applied Optics Congress 2021 (3D, COSI, DH, ISA, pcAOP)*, 2021, p. CTh4A.4, [Optica URL](#).
- [65] K. Itoh, “Analysis of the phase unwrapping algorithm,” *Applied Optics*, vol. 21, no. 14, pp. 2470–2470, 1982, [Optica URL](#).
- [66] Z. Mao, N. Chimitt, and S. H. Chan, “Accelerating atmospheric turbulence simulation via learned phase-to-space transform,” in *2021 IEEE/CVF International Conference on Computer Vision (ICCV)*, 2021, pp. 14739–14748, [IEEE Xplore](#).
- [67] N. Chimitt and S. H. Chan, “Simulating anisoplanatic turbulence by sampling intermodal and spatially correlated Zernike coefficients,” *Optical Engineering*, vol. 59, no. 8, pp. 083101, 2020, [SPIE URL](#).
- [68] N. Chimitt, X. Zhang, Z. Mao, and S. H. Chan, “Real-time dense field phase-to-space simulation of imaging through atmospheric turbulence,” *IEEE Transactions on Computational Imaging*, 2022, [IEEE Xplore](#).
- [69] J. R. Fienup, “Phase-retrieval algorithms for a complicated optical system,” *Applied Optics*, vol. 32, no. 10, pp. 1737–1746, 1993, [Optica URL](#).
- [70] B. Mildenhall, P. P. Srinivasan, M. Tancik, J. T. Barron, R. Ramamoorthi, and R. Ng, “Nerf: Representing scenes as neural radiance fields for view synthesis,” *Communications of the ACM*, vol. 65, no. 1, pp. 99–106, 2021, [ACM URL](#).